TOPOLOGICAL DERIVATIVE-BASED TOPOLOGY OPTIMIZATION OF PLATE STRUCTURES UNDER BENDING EFFECTS

F.S. CARVALHO, D. RUSCHEINSKY, S.M. GIUSTI, C.T.M. ANFLOR AND A.A. NOVOTNY

Abstract. In this work, the topological derivatives of L^2 and energy norms associated with the solution to Kirchhoff and Reissner-Mindlin plate bending models are introduced. Based on existing theoretical results, closed forms of the sensitivities are presented. A zero-order term is introduced in the equilibrium equations, which allows for adapting the obtained sensitivities to the context of topology optimization of plates under elastic support and free vibration condition as well. The resulting analytical formulae are used together with a level-set domain representation method to devise a simple topology design algorithm. Several finite element-based representative numerical experiments are presented showing its applications to the compliance minimization and eigenvalue maximization of Kirchhoff as well as Reissner-Mindlin plate structures under bending effects.

1. Introduction

Plates are structural elements where one of its dimensions, namely thickness, is much smaller than the others, contained in a plane. These elements are widely used in the naval, nuclear, aeronautical and civil industries, among others, due to their structural capability to cover large distances or surfaces. Based on the previous geometrical description, the mechanical behaviour of the structural element can be reduced to an analysis over the middle plane of the plate. Therefore, some hypothesis over the thickness must be made. The first theory introduced for plates was the classical thin plate theory of Kirchhoff (1850), where some assumptions were imposed by omitting the shear deformations and rotary inertia. In the papers by Reissner (1945) and Mindlin (1951), the shear deformations are considered and the rotation and lateral deflections are decoupled given arise to the Reissner-Mindlin theory, which allowed more accurate results in thick plate bending analysis. Since then, these theories have been widely and successfully used to analyse several structural problems modeled by plates in many engineering applications.

The theory of plates is a broad field and its optimal design can be analyzed from different engineering points of view. Regarding optimization of plates by considering as design variable the thickness (Kropiowska et al., 2019; Czarnecki and Lewiński, 2013), composite materials (Goo et al., 2016) and a formulation of Free Material Optimization (FMO) for laminated plates (Weldeyesus and Stolpe, 2016). In the paper by Leal and Soares (1989) was proposed a theory of design sensitivity analysis of structures based on mixed finite element models. The theory was developed to the sensitivity of the displacements and stresses of plates due to thickness variation. The sensitivity analysis was developed for static, dynamic and stability constraints based on mixed finite element models. The topology optimization applied for plates structures arise naturally due to the industrial demand to generate innovative design concepts that lead to weight savings and vibration control. The achievement of the best topology that attends the design criteria becomes crucial given rising for new technologies, materials, and high-end applications.

Date: July 31, 2020.

Key words and phrases. Optimal design of plates, topological derivative method, compliance minimization, eigenvalue maximization.

In recent years, the topology optimization methods have been object of attention and studied extensively. Beyond the classical problem of compliance minimization under volume constraint, maximization of the structural fundamental eigenvalue is the main problem in vibration control engineering, also playing an important role in machine design, automotive industry, and aerospace. A pioneered work based on topology optimization applied to eigenvalue problems was introduced by Diaaz and Kikuchi (1992), where a single frequency was considered in the optimization process. Since then, some important problems related to this subject have been treated and received important scientific attention, for instance, eigenfrequency maximization by considering the mixture of two elastic materials (Allaire et al., 2001), maximization of *performance index* by considering displacement and stress constraint (Liang et al., 2001; Liang, 2004), optimization of simple and multiple eigenvalues (Du and Olhoff, 2007), optimal design regarding to accurate geometric description (Li et al., 2010) and advances meshless and level-set methods (Khan et al., 2020).

The topological derivative, initially introduced by Sokolowski and Zochowski (1999), has been also successfully employed for topology optimization; and despite of being most frequently implemented with mesh methods it's also suitable for meshless methods (Neches and Cisilino, 2008; Hur et al., 2017; Anflor et al., 2018). In this sense, the topological derivative (TD) is a versatile method that can contribute significantly to the topology optimization field independently of the numerical or optimization method employed. The topological derivative gives the sensitive of a cost function when the domain under consideration is modified by the insertion of a singular perturbation, like of a hole, inclusion or even cracks. In fact, the TD is the main term of the asymptotic expansion of the selected cost function submitted to the differential governing equation as constraint (Novotny and Sokołowski, 2013; Novotny et al., 2019). Depending on the differential governing equation being considered, the derivation procedure becomes highly complex. Closed form of the TD can be obtained after an intensive analytical work. In this context, an available set of TD closed formulas for several classes of problems can contribute significantly in the topology optimization field once it can be coupled with diverse optimization methods available in the literature as aforementioned. The topological derivative derivation for the Kirchhoff plate bending problem considering the fourth-order differential operator was firstly considered in the paper by Novotny et al. (2005). Extension of that results by taking into account a general class of shape functionals was presented by Amstutz and Novotny (2011). In the paper by Turevsky et al. (2009) a numerical method to compute the first-order variation of some quantities of interest when an arbitrary-shaped features is introduced within the plate domain has been proposed. The topological derivative with respect to introduction of reinforcement in a plate was presented and discussed in details by Bojczuk and Mróz (2009). The topological derivative for an elliptical hole in bending plate model was obtained by Bojczuk and Mróz (2012). A detailed analysis of volume control methods for topological optimization of plate by using topological derivative concept was presented by Campeão et al. (2014). Later the topological derivative for the total potential energy associated with the Reissner-Mindlin plate bending problem was derived by Sales et al. (2015). The mechanical model leads a coupled system of second-order partial differential equations. How to deal with such a coupled system represents the main contribution of the authors. Therefore, the Kirchhoff plate model has already been extensively studied from both theoretical and numerical point of views. On the other hand, there are just few theoretical works dealing with Reissner-Mindlin plate model. In particular, only the energy shape functional has been considered and nothing can be found from the numerical point of view.

In the present work the topological derivatives of L^2 and energy norms associated with the solution to Kirchhoff and Reissner-Mindlin plate bending problems are presented.

A zero-order term is introduced in the equilibrium equations, which allows for adapting the obtained sensitivities to the context of topology optimization of plates under elastic support and free vibration condition as well. The resulting formulae are used together with a level-set domain representation method to devise a simple and efficient topology design algorithm. Some numerical experiments are presented showing its applications to the compliance minimization and eigenvalue maximization of Kirchhoff as well as Reissner-Mindlin plate structures.

The layout of the paper is as follows. In Section 2 the topological derivative is introduced for Kirchhoff (Section 2.1) and Reissner-Mindlin (Section 2.2) plate theories. The proof of the existence of the associated topological derivatives are presented, together with the resulting sensitivities of the L^2 and energy norms of the solutions to the problems under consideration. Section 3 presents some numerical examples in order to illustrate the validity and effectiveness of the present formulation, including application to compliance minimization (Section 3.1) and first eigenvalue maximization (Section 3.2). Finally, the paper ends with some concluding remarks in Section 4.

2. Topological Derivative

Let us consider an open and bounded domain $\Omega \subset \mathbb{R}^2$ which is subject to a nonsmooth perturbation confined in a small region $\omega_\varepsilon(\widehat{x})$ of size ε and center at $\widehat{x} \in \Omega$, with $\overline{\omega_\varepsilon} \subset \Omega$. We introduce a characteristic function $x \mapsto \chi(x)$ associated to the unperturbed domain, namely $\chi = \mathbb{1}_\Omega$ such that

$$|\Omega| = \int_\Omega \chi, \tag{2.1}$$

where $|\Omega|$ is the Lebesgue measure of Ω. Then, we define a characteristic function associated to the topologically perturbed domain of the form $x \mapsto \chi_\varepsilon(\widehat{x}, x)$. In the case of a perforation, for instance $\chi_\varepsilon(\widehat{x}) = \mathbb{1}_\Omega - \mathbb{1}_{\omega_\varepsilon(\widehat{x})}$ and the singularly perturbed domain is given by $\Omega_\varepsilon = \Omega \setminus \overline{\omega_\varepsilon}$. Then, we assume that a given shape functional $\psi(\chi_\varepsilon(\widehat{x}))$, associated to the topologically perturbed domain, admits the following topological asymptotic expansion

$$\psi(\chi_\varepsilon(\widehat{x})) = \psi(\chi) + f(\varepsilon) D_T \psi(\widehat{x}) + o(f(\varepsilon)), \tag{2.2}$$

where $\psi(\chi)$ is the shape functional associated to the unperturbed domain, $f(\varepsilon)$ is a positive function such that $f(\varepsilon) \to 0$ with $\varepsilon \to 0^+$ and $o(f(\varepsilon))$ is the remainder. The function $\widehat{x} \mapsto D_T \psi(\widehat{x})$ is called the topological derivative of ψ at $\widehat{x}$. Therefore, this derivative can be seen as a first order correction of $\psi(\chi)$ to approximate $\psi(\chi_\varepsilon(\widehat{x}))$.

The topological derivatives of the L^2 and energy norms associated with the Kirchhoff and Reissner-Mindlin plate models, with respect to the nucleation of circular inclusions, are presented in this section. The mathematical models for both problems as well as the respective shape functionals we are dealing with are introduced. The original unperturbed and topologically perturbed problems are stated, together with arguments on the existence of the associated topological derivatives. In particular, we show that a class of $H^2(\Omega;\mathbb{R})$ and $H^1(\Omega;\mathbb{R}^2) \times H^1(\Omega;\mathbb{R})$ shape functional (including the energy shape functional), respectively associated with Kirchhoff and Reissner-Mindlin problems, is continuous with respect to the small parameter ε, and thus differentiable in the sense of (2.2). Finally, the resulting topological derivatives are presented in their close forms, which are useful for engineering applications.

We start by introducing the kinematic assumptions of each plate bending problem we are dealing with. It is assumed that the plates are submitted to bending effects. In addition, the plates are represented by a two-dimensional domain $\Omega \subset \mathbb{R}^2$ with thickness $h > 0$ supposed to be constant. The domain Ω is divided into two subdomains $\omega \subset \Omega$ and the complement $\Omega \setminus \omega$. Finally, let us introduce a set of piecewise constant functions α, β, ρ and f as presented in Table 1.

TABLE 1. Values of α, β, ρ and f.

	α	β	ρ	f
$\Omega \setminus \omega$	α_0	β_0	ρ_0	f_0
ω	α_1	β_1	ρ_1	f_1

The topological perturbation is given by the nucleation of a small circular inclusion of the form $\omega_\varepsilon(\widehat{x}) := B_\varepsilon(\widehat{x}) = \{\|x - \widehat{x}\| < \varepsilon\}$ for $\widehat{x} \in \Omega$. In particular, the perturbation is governed by a set of piecewise constant functions α_ε, β_ε, ρ_ε and f_ε according to Table 2 and Table 3.

TABLE 2. Values of α_ε, β_ε, ρ_ε and f_ε.

	α_ε	β_ε	ρ_ε	f_ε
$\Omega \setminus B_\varepsilon$	α	β	ρ	f
B_ε	$\gamma_\alpha\alpha$	$\gamma_\beta\beta$	$\gamma_\rho\rho$	$\gamma_f f$

TABLE 3. Values of γ_α, γ_β, γ_ρ and γ_f.

	γ_α	γ_β	γ_ρ	γ_f
$\Omega \setminus \omega$	α_1/α_0	β_1/β_0	ρ_1/ρ_0	f_1/f_0
ω	α_0/α_1	β_0/β_1	ρ_0/ρ_1	f_0/f_1

Before starting the main results of this section, let us introduce the following fourth-order polarization tensor associated with the plate bending model

$$\mathbb{P} = -\frac{1-\gamma_\alpha}{1+\gamma_\alpha\delta_2}\left((1+\delta_2)\mathbb{I} + \frac{1-\gamma_\alpha}{2}\frac{\delta_1-\delta_2}{1+\gamma_\alpha\delta_1}\mathrm{I}\otimes\mathrm{I}\right), \tag{2.3}$$

where constants δ_1 and δ_2 will be defined later according to the model problem we are dealing with, namely Kirchhoff or Reissner-Mindlin. In (2.3), the symbols I and $\mathbb{I}$ are used to denote the second and fourth order identity tensors, respectively

2.1. **Kirchhoff problem.** The theory of Kirchhoff bending plates is based on the following kinematic assumption:

> *The normal fibers to the middle plane of the plate remain normal during deformation and do not suffer variations in their length. Consequently, both transversal shear and normal deformations are null.*

Therefore, the original unperturbed problem can be stated as: Find $u \in \mathcal{V}(\Omega)$, such that

$$\int_\Omega \alpha M(u)\cdot\nabla\nabla v + \int_\Omega \rho k u v = \int_\Omega f v, \quad \forall v \in \mathcal{V}(\Omega), \tag{2.4}$$

where $\mathcal{V}(\Omega) = H_0^2(\Omega;\mathbb{R})$. The coefficients α, ρ and f are given in Table 1. In addition, $M(u) = \mathbb{C}\nabla\nabla u$ is the moment tensor, $u : \Omega \mapsto \mathbb{R}$ the transverse displacement and k a positive function. The constitutive tensor $\mathbb{C}$ is given by

$$\mathbb{C} = \frac{Eh^3}{12(1-\nu^2)}\left((1-\nu)\mathbb{I} + \nu\mathrm{I}\otimes\mathrm{I}\right), \tag{2.5}$$

being ν is the Poisson ratio, E is the Young modulus and h the plate thickness. The L^2 and energy norms shape functionals, we are dealing with, are respectively defined as

$$\mathcal{G}(u) = \int_\Omega \rho k|u|^2 \qquad \text{and} \qquad \mathcal{J}(u) = \int_\Omega \alpha M(u)\cdot\nabla\nabla u. \tag{2.6}$$

In order to simplify the form of the topological derivatives, we introduce the adjoint problems for displacements q and p, as

$$q \in \mathcal{V}(\Omega) : \int_\Omega \alpha M(q) \cdot \nabla\nabla v + \int_\Omega \rho k q v = -2 \int_\Omega \rho k u v, \quad \forall v \in \mathcal{V}(\Omega), \tag{2.7}$$

$$p \in \mathcal{V}(\Omega) : \int_\Omega \alpha M(p) \cdot \nabla\nabla v + \int_\Omega \rho k p v = -2 \int_\Omega \alpha M(u) \cdot \nabla\nabla v, \quad \forall v \in \mathcal{V}(\Omega). \tag{2.8}$$

The topologically perturbed counterpart of problem (2.4) is written as: Find $u_\varepsilon \in \mathcal{V}(\Omega)$, such that

$$\int_\Omega \alpha_\varepsilon M(u_\varepsilon) \cdot \nabla\nabla v + \int_\Omega \rho_\varepsilon k u_\varepsilon v = \int_\Omega f_\varepsilon v, \quad \forall v \in \mathcal{V}(\Omega), \tag{2.9}$$

where the coefficients α_ε, ρ_ε and f_ε are defined through Table 2 and Table 3. The associated shape functionals are then defined as

$$\mathcal{G}_\varepsilon(u_\varepsilon) = \int_\Omega \rho_\varepsilon k |u_\varepsilon|^2 \qquad \text{and} \qquad \mathcal{J}_\varepsilon(u_\varepsilon) = \int_\Omega \alpha_\varepsilon M(u_\varepsilon) \cdot \nabla\nabla u_\varepsilon. \tag{2.10}$$

2.1.1. *Existence of the topological derivative.* The shape functionals in the original and perturbed domains are respectively introduced through equations (2.4) and (2.9). Now, it is possible to state the following result ensuring the existence of the associated topological derivatives:

Lemma 1. *Let u and u_ε be solutions to the original* (2.4) *and perturbed* (2.9) *problems, respectively. Then the estimate $\|u_\varepsilon - u\|_{H^2(\Omega;\mathbb{R})} = O(\varepsilon)$ holds true.*

Proof. Let us subtract (2.4) from (2.9). By setting $v = u_\varepsilon - u$ as test function, after some simple manipulations there is

$$\begin{aligned} \int_\Omega \alpha_\varepsilon M(u_\varepsilon - u) \cdot \nabla\nabla(u_\varepsilon - u) + \int_\Omega \rho_\varepsilon k \|u_\varepsilon - u\|^2 = \\ \int_{B_\varepsilon} (1-\gamma_\alpha) \alpha M(u) \cdot \nabla\nabla(u_\varepsilon - u) + \int_{B_\varepsilon} (1-\gamma_\rho) \rho k u (u_\varepsilon - u) \\ - \int_{B_\varepsilon} (1-\gamma_f) f (u_\varepsilon - u). \end{aligned} \tag{2.11}$$

where we have taken into account the contrasts reported in Table 2 and Table 3. The Cauchy-Schwarz inequality yield

$$\int_\Omega \alpha_\varepsilon M(u_\varepsilon - u) \cdot \nabla\nabla(u_\varepsilon - u) + \int_\Omega \rho_\varepsilon k \|u_\varepsilon - u\|^2 \leqslant C_1 \varepsilon \|u_\varepsilon - u\|_{H^2(\Omega;\mathbb{R})}, \tag{2.12}$$

where we have used the elliptic regularity of function u. From the coercivity of the bilinear form on the left-hand side of the above inequality, we have

$$c \|u_\varepsilon - u\|^2_{H^2(\Omega;\mathbb{R})} \leqslant \int_\Omega \alpha_\varepsilon M(u_\varepsilon - u) \cdot \nabla\nabla(u_\varepsilon - u) + \int_\Omega \rho_\varepsilon k \|u_\varepsilon - u\|^2, \tag{2.13}$$

which leads to the result

$$\|u_\varepsilon - u\|_{H^2(\Omega;\mathbb{R})} \leqslant C\varepsilon, \tag{2.14}$$

with the constant $C = C_1/c$ independent of the small parameter ε. □

2.1.2. *Topological sensitivities.* By setting the constants δ_1 and δ_2 in the definition of the polarization tensor (2.3) as follows

$$\delta_1 = \frac{1+\nu}{1-\nu} \quad \text{and} \quad \delta_2 = \frac{1-\nu}{3+\nu}, \tag{2.15}$$

we can state the two main results of this Section, whose proofs are completely analogous to the presented by Amstutz and Novotny (2011):

Theorem 2. *Let $\mathcal{G}(u)$ be the shape functional defined by (2.6)-left, then its associated topological derivative is given by*

$$D_T\mathcal{G} = \alpha\mathbb{P}M(u)\cdot\nabla\nabla q - (1-\gamma_\rho)\rho k u(u+q) + (1-\gamma_f)fq \quad a.e.\ in\,\Omega \tag{2.16}$$

where q is the adjoint state solution of (2.7).

Theorem 3. *Let $\mathcal{J}(u)$ be the shape functional presented in (2.6)-right, then its topological derivative is given by*

$$D_T\mathcal{J} = \alpha\mathbb{P}M(u)\cdot\nabla\nabla(u+p) - (1-\gamma_\rho)\rho k u p + (1-\gamma_f)fp \quad a.e.\ in\,\Omega \tag{2.17}$$

where p is the adjoint solution of problem (2.8).

2.2. **Reissner-Mindlin problem.** The theory of Reissner-Mindlin bending plates is based on the following kinematic assumption:

> *The normal fibers to the middle plane of the plate remain straight during the deformation process and do not suffer variations in their length, but they do not necessarily remain normal to the middle plane. Consequently, the transversal shear deformations are not negligible and the normal deformations are null.*

Therefore, the unperturbed problem is stated as: Find $(\theta, u) \in \mathcal{H}(\Omega)$, such that

$$\int_\Omega \alpha M(\theta)\cdot(\nabla\eta)^s + \int_\Omega \beta Q(\theta,u)\cdot(\eta-\nabla v) + \int_\Omega \rho k u v = \int_\Omega fv, \quad \forall\,(\eta,v)\in\mathcal{H}(\Omega), \tag{2.18}$$

where $\mathcal{H}(\Omega) = H_0^1(\Omega;\mathbb{R}^2)\times H_0^1(\Omega;\mathbb{R})$. The coefficients α, β, ρ and f are given in Table 1. In addition, $\theta : \Omega \mapsto \mathbb{R}^2$ is the rotation, $u : \Omega \mapsto \mathbb{R}$ is the transversal displacement, $M(\theta) = \mathbb{C}(\nabla\theta)^s$ is the generalized bending moment tensor and $Q(\theta,u) = D(\theta - \nabla u)$ is the generalized shear tensor. The constitutive tensor $\mathbb{C}$ is defined by (2.5) whereas the second order tensor D is given by

$$D = \frac{\sigma E h}{2(1+\nu)}\mathrm{I}, \tag{2.19}$$

with shear correction factor $\sigma = 5/6$. The L^2 and energy norms shape functionals, we are dealing with, are defined as

$$\mathcal{G}(\theta,u) = \int_\Omega \rho k|u|^2 \quad \text{and} \quad \mathcal{J}(\theta,u) = \int_\Omega (\alpha M(\theta)\cdot(\nabla\theta)^s + \beta Q(\theta,u)\cdot(\theta-\nabla u)). \tag{2.20}$$

In order to simplify the form of the topological derivatives, we introduce the adjoint problems for displacements (q,p) and the rotations (φ,ϕ), as

$$(\varphi,q)\in\mathcal{H}(\Omega) : \int_\Omega \alpha M(\varphi)\cdot(\nabla\eta)^s + \int_\Omega \beta Q(\varphi,q)\cdot(\eta-\nabla v) + \int_\Omega \rho k q v = \\ -2\int_\Omega \rho k u v, \quad \forall(\eta,v)\in\mathcal{H}(\Omega), \tag{2.21}$$

$$(\phi,p)\in\mathcal{H}(\Omega):\int_\Omega \alpha M(\phi)\cdot(\nabla\eta)^s+\int_\Omega \beta Q(\phi,p)\cdot(\eta-\nabla v)+\int_\Omega \rho k p v=$$
$$-2\int_\Omega(\alpha M(\theta)\cdot(\nabla\eta)^s+\beta Q(\theta,u)\cdot(\eta-\nabla v)),\quad \forall(\eta,v)\in\mathcal{H}(\Omega). \quad (2.22)$$

The topologically perturbed counterpart of problem (2.18) is written as: Find $(\theta_\varepsilon,u_\varepsilon)\in\mathcal{H}(\Omega)$, such that

$$\int_\Omega \alpha_\varepsilon M(\theta_\varepsilon)\cdot(\nabla\eta)^s+\int_\Omega \beta_\varepsilon Q(\theta_\varepsilon,u_\varepsilon)\cdot(\eta-\nabla v)+\int_\Omega \rho_\varepsilon k u_\varepsilon v=\int_\Omega f_\varepsilon v,\quad \forall\,(\eta,v)\in\mathcal{H}(\Omega), \quad (2.23)$$

where the coefficients α_ε, β_ε, ρ_ε and f_ε are reported in Table 2 and Table 3. The associated shape functionals are then defined as

$$\mathcal{G}_\varepsilon(\theta_\varepsilon,u_\varepsilon) = \int_\Omega \rho_\varepsilon k|u_\varepsilon|^2 \qquad \text{and} \quad (2.24)$$
$$\mathcal{J}_\varepsilon(\theta_\varepsilon,u_\varepsilon) = \int_\Omega(\alpha_\varepsilon M(\theta_\varepsilon)\cdot(\nabla\theta_\varepsilon)^s+\beta_\varepsilon Q(\theta_\varepsilon,u_\varepsilon)\cdot(\theta_\varepsilon-\nabla u_\varepsilon)). \quad (2.25)$$

2.2.1. *Existence of the topological derivative.* The shape functionals in the original and perturbed domains are defined by equations (2.18) and (2.23), respectively. Therefore, the existence of the topological derivatives associated with the problems we are dealing with are ensured by the following important result:

Lemma 4. *Let (θ,u) and $(\theta_\varepsilon,u_\varepsilon)$ be solutions to problems* (2.18) *and* (2.23)*, respectively. Then, the estimates $\|\theta_\varepsilon-\theta\|_{H^1(\Omega;\mathbb{R}^2)}=O(\varepsilon)$ and $\|u_\varepsilon-u\|_{H^1(\Omega;\mathbb{R})}=O(\varepsilon)$ hold true.*

Proof. Let us is subtract (2.18) from (2.23) to obtain

$$\int_\Omega \alpha_\varepsilon M(\widetilde{\theta}_\varepsilon)\cdot(\nabla\eta)^s+\int_\Omega \beta_\varepsilon Q(\widetilde{\theta}_\varepsilon,\widetilde{u}_\varepsilon)\cdot(\eta-\nabla v)+\int_\Omega \rho_\varepsilon k\widetilde{u}_\varepsilon v=$$
$$\int_{B_\varepsilon}(1-\gamma_\alpha)\alpha M(\theta)\cdot(\nabla\eta)^s+\int_{B_\varepsilon}(1-\gamma_\beta)\beta Q(\theta,u)\cdot(\eta-\nabla v)$$
$$+\int_{B_\varepsilon}(1-\gamma_\rho)\rho k u v-\int_{B_\varepsilon}(1-\gamma_f)fv, \quad (2.26)$$

where we have introduced the notations $\widetilde{\theta}_\varepsilon=\theta_\varepsilon-\theta$ and $\widetilde{u}_\varepsilon=u_\varepsilon-u$. By setting $\eta=\widetilde{\theta}_\varepsilon$ and $v=\widetilde{u}_\varepsilon$ as test functions in the above equation, the Cauchy-Schwarz inequality together with the triangular inequality, yield

$$\int_\Omega \alpha_\varepsilon M(\widetilde{\theta}_\varepsilon)\cdot(\nabla\widetilde{\theta}_\varepsilon)^s+\int_\Omega \beta_\varepsilon Q(\widetilde{\theta}_\varepsilon,\widetilde{u}_\varepsilon)\cdot(\widetilde{\theta}_\varepsilon-\nabla\widetilde{u}_\varepsilon)+\int_\Omega \rho_\varepsilon k|\widetilde{u}_\varepsilon|^2\le$$
$$C_1\varepsilon\left(\|\widetilde{\theta}_\varepsilon\|_{H^1(\Omega;\mathbb{R}^2)}+\|\widetilde{u}_\varepsilon\|_{H^1(\Omega;\mathbb{R})}\right), \quad (2.27)$$

where we have considered the elliptic regularity of functions θ and u. Finally, from the coercivity of the bilinear form on the left-hand side of the above inequality, namely

$$c\left(\|\widetilde{\theta}_\varepsilon\|^2_{H^1(\Omega;\mathbb{R}^2)}+\|\widetilde{u}_\varepsilon\|^2_{H^1(\Omega;\mathbb{R})}\right)\le\int_\Omega \alpha_\varepsilon M(\widetilde{\theta}_\varepsilon)\cdot(\nabla\widetilde{\theta}_\varepsilon)^s$$
$$+\int_\Omega \beta_\varepsilon Q(\widetilde{\theta}_\varepsilon,\widetilde{u}_\varepsilon)\cdot(\widetilde{\theta}_\varepsilon-\nabla\widetilde{u}_\varepsilon)+\int_\Omega \rho_\varepsilon k|\widetilde{u}_\varepsilon|^2, \quad (2.28)$$

we have that

$$\frac{c}{2}\left(\|\widetilde{\theta}_\varepsilon\|_{H^1(\Omega;\mathbb{R}^2)}+\|\widetilde{u}_\varepsilon\|_{H^1(\Omega;\mathbb{R})}\right)^2 \leq c\left(\|\widetilde{\theta}_\varepsilon\|^2_{H^1(\Omega;\mathbb{R}^2)}+\|\widetilde{u}_\varepsilon\|^2_{H^1(\Omega;\mathbb{R})}\right) \leq C_1\varepsilon\left(\|\widetilde{\theta}_\varepsilon\|_{H^1(\Omega;\mathbb{R}^2)}+\|\widetilde{u}_\varepsilon\|_{H^1(\Omega;\mathbb{R})}\right). \quad (2.29)$$

Finally, it follows immediately

$$\|\widetilde{\theta}_\varepsilon\|_{H^1(\Omega;\mathbb{R}^2)}+\|\widetilde{u}_\varepsilon\|_{H^1(\Omega;\mathbb{R})} \leq C\varepsilon, \quad (2.30)$$

with the constant $C = 2C_1/c$ independent of the small parameter ε. □

2.2.2. *Topological sensitivities.* Let us introduce the following second-order tensor

$$P = -2\frac{1-\gamma_\beta}{1+\gamma_\beta}\,\mathrm{I}. \quad (2.31)$$

Now, by setting the constants δ_1 and δ_2 in the definition of the polarization tensor (2.3) as follows

$$\delta_1 = \frac{1+\nu}{1-\nu} \quad \text{and} \quad \delta_2 = \frac{3-\nu}{1+\nu}, \quad (2.32)$$

we can state the two main results of this section, whose proofs are completely analogous to the paper by Sales et al. (2015):

Theorem 5. *Let $\mathcal{G}(\theta,u)$ be the shape functional defined by* (2.20)*-left, then its associated topological derivative is given by*

$$D_T\mathcal{G} = \alpha\mathbb{P}M(\theta)\cdot(\nabla\varphi)^s + \beta PQ(\theta,u)\cdot(\varphi-\nabla q) - (1-\gamma_\rho)\rho ku(u+q) + (1-\gamma_f)fq \quad a.e.\ in\,\Omega \quad (2.33)$$

where (φ,q) is the adjoint state solution of (2.21).

Theorem 6. *Let $\mathcal{J}(\theta,u)$ be the shape functional presented in* (2.20)*-right, then its associated topological derivative is given by*

$$D_T\mathcal{J} = \alpha\mathbb{P}M(\theta)\cdot(\nabla(\theta+\phi))^s + \beta PQ(\theta,u)\cdot((\theta+\phi)-\nabla(u+p)) - (1-\gamma_\rho)\rho kup + (1-\gamma_f)fp \quad a.e.\ in\,\Omega \quad (2.34)$$

where (ϕ,p) is the adjoint solution of problem (2.22).

3. Representative Numerical Examples

The topological derivatives of the L^2 and energy norms of the solutions of Kirchhoff and Reissner-Mindlin problems, with respect to nucleation of inclusions endowed with different material properties of the background, have been presented in the previous section. Now, some selected examples are considered, showing applications in the context of compliance minimization and eigenvalue maximization.

The hold-all domain is represented by $\Omega \subset \mathbb{R}^2$. We assume that the strong phase is represented by $\mathcal{D} := \Omega \setminus \omega$, so that $\omega \subset \Omega$ represents the weak phase used to mimic holes. By using the linear penalty method for volume control, the optimization problem we are dealing with can be stated as follows:

$$\underset{\mathcal{D}\subset\Omega}{\text{Minimize}}\; J_\mu(\mathcal{D}) = \frac{J(\mathcal{D})}{J(\Omega)} + \mu\frac{|\mathcal{D}|}{|\Omega|}\,, \quad (3.1)$$

subject to (2.4) or (2.18), where $J(\mathcal{D})$ and $|\mathcal{D}|$ are the shape functional and volume evaluated at the variable domain $\mathcal{D}$, whereas $J(\Omega)$ and $|\Omega|$ are their associated counterparts evaluated at the (fixed) hold-all domain Ω. In the optimization problem introduced in equation (3.1), $\mu > 0$ is a fixed multiplier that imposes a restriction on the volume of elastic material. The minimization problem (3.1) is solved by using a topology optimization

algorithm based on the topological derivative together with a level-set domain representation method (Amstutz and Andrä, 2006). For the sake of completeness, let us explain briefly the main ideas. A locally sufficient optimality condition, under the considered class of domain perturbation given by circular inclusions, can be stated as (Amstutz, 2011b):

$$D_T J_\mu(x) > 0 \quad \forall x \in \Omega. \tag{3.2}$$

Let us introduce a level-set domain representation function $\Psi \in L^2(\Omega)$ of the form:

$$\mathcal{D} = \{\Psi(x) < 0, \text{ for } x \in \Omega\}, \tag{3.3}$$

$$\omega = \{\Psi(x) > 0, \text{ for } x \in \Omega\}, \tag{3.4}$$

where Ψ vanishes on the interface $\partial\omega$. We define the quantity

$$g(x) := \begin{cases} -D_T J_\mu(x), & \text{if } \Psi(x) < 0, \\ +D_T J_\mu(x), & \text{if } \Psi(x) > 0. \end{cases} \tag{3.5}$$

The topological derivative of the volume constraint is trivially given by $D_T|\mathcal{D}| = -1$ in $\Omega \setminus \omega$ and $D_T|\mathcal{D}| = +1$ in ω. On the other hand, the topological derivative of the shape functional $J(\mathcal{D})$ has to be evaluated in $\Omega\setminus\omega$ and ω according to the values for the contrasts summarized through Table 3. The above equation allows for rewriting the condition (3.2) in the following equivalent form

$$\begin{cases} g(x) < 0, & \text{if } \Psi(x) < 0, \\ g(x) > 0, & \text{if } \Psi(x) > 0. \end{cases} \tag{3.6}$$

Note that (3.6) is satisfied whenever quantity g coincides with level-set function Ψ up to a strictly positive number. Thus, the basic idea consists in finding a fixed point satisfying the following condition

$$\tau > 0 : g = \tau\Psi. \tag{3.7}$$

Therefore,

$$\delta := \arccos\left[\frac{\langle g, \Psi\rangle_{L^2(\Omega)}}{\|g\|_{L^2(\Omega)}\|\Psi\|_{L^2(\Omega)}}\right] = 0, \tag{3.8}$$

which shall be used as optimality condition in the topology design algorithm, where δ is the angle between the functions g and Ψ in $L^2(\Omega)$.

Let us now explain the algorithm. We first choose an initial level-set function $\Psi^0 \in L^2(\Omega)$. In a generic iteration i, we compute function g^i associated with the level-set function $\Psi^i \in L^2(\Omega)$. Thus, the new level-set function Ψ^{i+1} is updated according to the following linear combination between the functions g^i and Ψ^i, explicitly given by

$$\Psi^{i+1} = \frac{1}{\sin(\delta^i)}\left[\sin((1-\kappa)\delta^i)\Psi^i + \sin(\kappa\delta^i)\frac{g^i}{\|g^i\|_{L^2(\Omega)}}\right], \tag{3.9}$$

where δ^i is the angle between g^i and Ψ^i according to (3.8), and κ is a step size determined by a line-search performed in order to decrease the value of the objective function J_μ^i associated with Ψ^i. The step size κ is chosen at first as 1 and it is decreasing accordingly to $\kappa \leftarrow \kappa/2$ until the condition $J_\mu^i < J_\mu^{i-1}$ is fulfilled. The process ends when the condition $\delta^i \leq \epsilon_\delta$ is satisfied at some iteration, where ϵ_δ is a given small numerical tolerance. If at some iteration the line-search step size κ is found to be smaller then a given numerical tolerance $\epsilon_\kappa > 0$ and the optimality condition is not satisfied, namely $\delta_i > \epsilon_\delta$, then a mesh refinement of the hold-all domain Ω is carried out and the iterative process is continued.

In all numerical examples, the stopping criterion and the optimality threshold are given respectively by $\epsilon_\delta = 3^\circ$ and $\epsilon_\kappa = 10^{-3}$. In addition, the domain is discretized by using linear triangular finite elements resulting in an initial uniform mesh with $14,400$ elements and $7,321$ nodes. In order to increase the accuracy as well as the topology smoothness

3 steps of uniform mesh refinement during the iterative process are allowed, leading to a mesh with $921,600$ elements and $461,761$ nodes.

3.1. **Compliance minimization.** The compliance of the plate under bending effects is obtained as the sum of the shape functionals given by (2.6) for Kirchhoff problem and by (2.20) for Reissner-Mindlin problem. The zero order term in both problems (see eqs. (2.4) and (2.18)) can be interpreted as an elastic support, so that we define the quantity $s = \rho k$, where s represents the stiffness of the support. The transverse load f is assumed to be fixed, so that its associated contrast $\gamma_f = 1$.

In the case of Kirchhoff plate bending problem, the shape functional to be minimized is defined as $J(\mathcal{D}) := \mathcal{J}(u) + \mathcal{G}(u)$, with $\mathcal{J}(u)$ and $\mathcal{G}(u)$ given by (2.6), where u is the solution to: Find u, such that

$$\left\{ \begin{array}{rcl} \operatorname{div}\operatorname{div}(\alpha M(u)) + su &=& f \quad \text{in} \quad \Omega, \\ u = \partial_n u &=& 0 \quad \text{on} \quad \partial\Omega. \end{array} \right. \tag{3.10}$$

Therefore, from Theorem 2 and Theorem 3, we have that the associated topological derivative of the compliance shape functional $J(\mathcal{D})$ is given by

$$D_T J = -\alpha \mathbb{P} M(u) \cdot \nabla\nabla u + (1 - \gamma_\rho) s |u|^2. \tag{3.11}$$

Analogously, in the case of Reissner-Mindlin plate bending problem, the shape functional to be minimized is defined as $J(\mathcal{D}) := \mathcal{J}(\theta, u) + \mathcal{G}(\theta, u)$, with $\mathcal{J}(\theta, u)$ and $\mathcal{G}(\theta, u)$ given by (2.20), where (θ, u) are the solutions to: Find (θ, u), such that

$$\left\{ \begin{array}{rcl} -\operatorname{div}(\alpha M(\theta)) + \beta Q(\theta, u) &=& 0 \quad \text{in} \quad \Omega\,, \\ \operatorname{div}(\beta Q(\theta, u)) + su &=& f \quad \text{in} \quad \Omega\,, \\ \theta = 0,\ u &=& 0 \quad \text{on} \quad \partial\Omega\,. \end{array} \right. \tag{3.12}$$

Thus, from Theorem 5 and Theorem 6, we have that the associated topological derivative of the compliance shape functional $J(\mathcal{D})$ is given by

$$D_T J = -\alpha \mathbb{P} M(\theta) \cdot (\nabla\theta)^s - \beta P Q(\theta, u) \cdot (\theta - \nabla u) + (1 - \gamma_\rho) s |u|^2. \tag{3.13}$$

In the numerical experiment we consider for both problems (Kirchhoff and Reissner-Mindlin) a hold-all domain Ω given by a clamped square of dimensions $(0,1) \times (0,1)\text{m}^2$ submitted to concentrated forces, perpendicular to the plane of the plate, of values $f = -1\text{MN}$ located at the centre of each plate quadrant. A circular elastic support of radius 0.2m and center at $(0.50, 0.50)$ is also considered (see sketch in Fig. 1). The concentrated loads are represented by black dots whereas the support is represented by a hatched circular area in grey color. The Young modulus is $E = 210\text{GPa}$, Poisson ratio $\nu = 0.3$, the stiffness of the elastic support is $s = 10^{-2}E$ and the plate thickness is $h = 0.05\text{m}$. The contrasts are given by $\gamma_\alpha = \gamma_\rho = 10^{-4}$ and the penalty parameter is set as $\mu = 1.7$. The experiments are labeled as Cases K1 and K2 for Kirchhoff with and without support, respectively, and Cases R1 and R2 for Reissner-Mindlin with and without support, respectively. The final topologies are presented in Fig. 2 and Fig. 3 for Kirchhoff (Cases K1 and K2) and Reissner-Mindlin (Cases R1 and R2) plates, respectively. Finally, the history of the compliance, volume fraction and shape function obtained during the iterative process are presented in Fig. 4 to Fig. 6.

In spite of the offset, a similar behavior between curves obtained for Kirchhoff plates can be observed for compliance, volume and shape function histories (see Cases K1 and K2 in Fig. 4 to Fig. 6). The same remark can be done regarding the Reissner-Mindlin curves (see Cases R1 and R2 in Fig. 4 to Fig. 6) suggesting a good convergence. In this sense, it can be seen that the differences in the final topologies resulted from both theories were driven by the influence of the elastic support. In the case of Reissner-Mindlin plates (Cases R1 and R2), it is also interesting to note that the energy in Fig. 4 increases

once the mesh is refined. This phenomenon can be explained by the transverse shear deformations, which allow for capturing the concentrated load effects, so that it is not observed in the case of Kirchhoff plates (Cases K1 and K2), as expected.

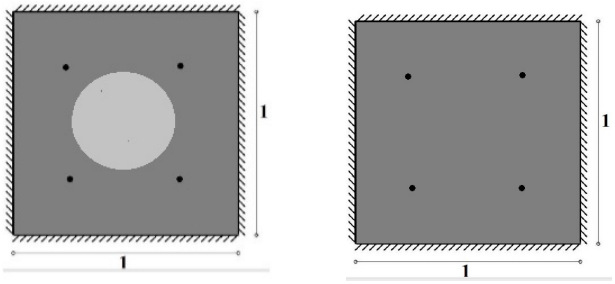

(a) with support (b) without support

FIGURE 1. Initial domain with support (a) and without support (b). The concentrated loads are represented by black dots whereas the elastic support is represented by a hatched circular area in grey color.

.

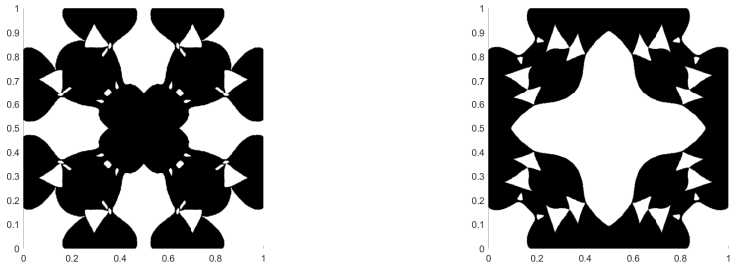

(a) Case K1 (b) Case K2

FIGURE 2. Final topologies for the Kirchhoff problem with support (a) and without support (b).

.

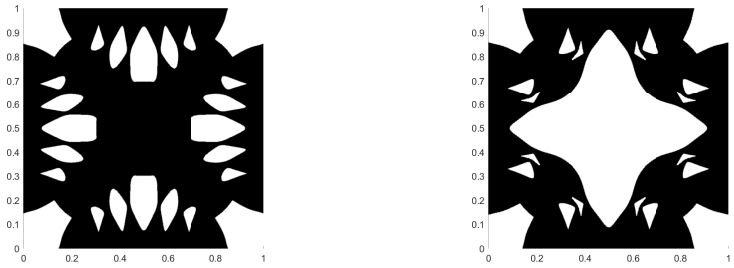

(a) Case R1 (b) Case R2

FIGURE 3. Final topologies for the Reissner-Mindlin problem with support (a) and without support (b).

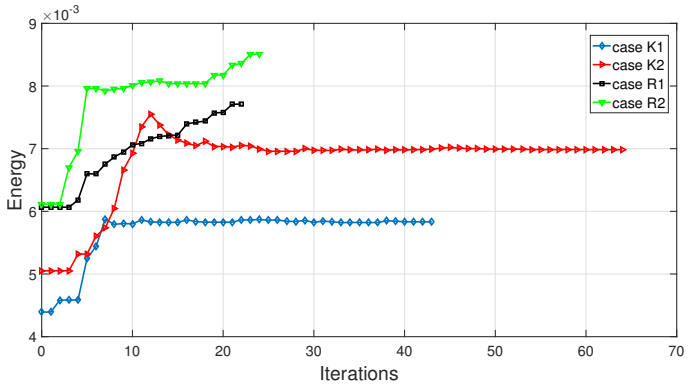

FIGURE 4. Compliance history.

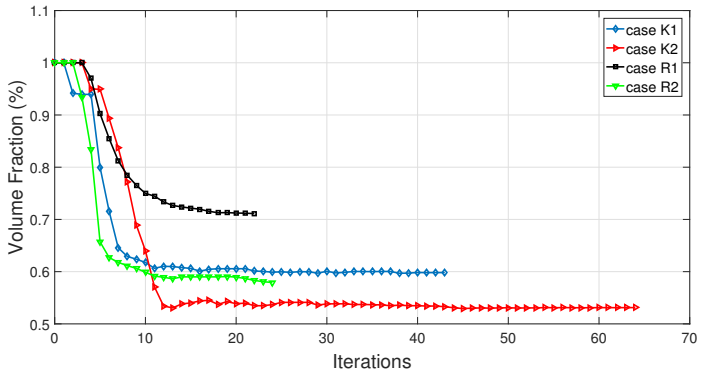

FIGURE 5. Volume fraction history.

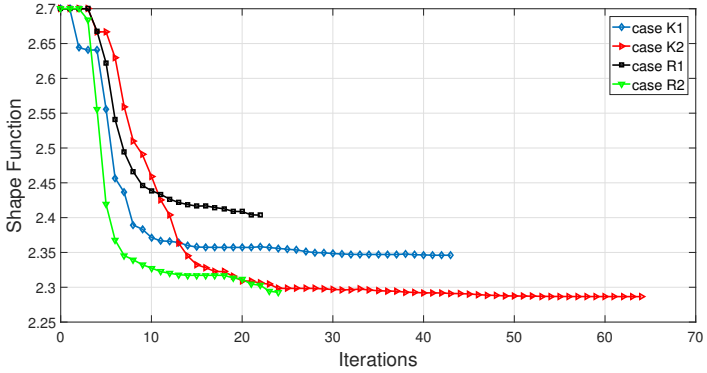

FIGURE 6. Shape function history.

3.2. **First eigenvalue maximization.** The topological derivative for simple eigenvalues of the Laplacian can be found in the paper by Ammari and Khelifi (2003). The extension to multiple eigenvalues and other types of problems has been derived by Nazarov and Sokołowski (2008). In particular, since the topological derivative obeys the basic rules of the Differential Calculus (including the quotient rule for differentiation), the topological sensitivity of the first eigenvalue associated with the Kirchhoff as well as Reissner-Mindlin plate bending problems can be formally derived from Theorems 2-3 and Theorems 5-6, respectively. The rigorous justification for these kind of results can be found in the book by (Novotny and Sokołowski, 2013, Ch 9). See also the paper by Amstutz (2011a) where the topological derivative for the first eigenvalue in a two-dimensional elasticity setting

was derived by using similar procedure. As observed by Haftka and Gürdal (1992), standard sensitivities of eigenvalues hold only in the case of distinct eigenvalues. According to Seyranian et al. (1994) symmetric and complex structures that depend on many design parameters often present multiple eigenvalues. A numerical method of solution was developed by the authors to determine an ascent direction in the design space for the smallest eigenvalue. More recently, a simple strategy proposed by Zhang et al. (2015) can be used in order to deal with multiplicity of eigenmodes, which consists in select the closest eigenmode to the current one. In the paper by Torii and Rocha de Faria (2017) a more sophisticated approach based on a smooth p-norm approximation for the smallest eigenvalue is presented. On the other hand, it is well-known that there exists a connection between the compliance minimization and first eigenfrequency maximization. In both cases, the optimal solutions, when they do exist, are given by the stiffer structure in view of the available amount of material. However, due to the intrinsic complex nature of such shape optimization problems, the optimal solutions for compliance minimization and first eigenvalue maximization may differ between them. In particular, in this section we propose a formulation specifically designed for dealing with first eigenvalue maximization problem.

The eigenvalue problem for the Kirchhoff model of a clamped thin plate under free vibration can be stated as: Find u and λ, such that

$$\left\{\begin{array}{rcll} \operatorname{div}\operatorname{div}(\alpha M(u)) &=& \lambda\rho u & \text{in} \quad \Omega, \\ u = \partial_n u &=& 0 & \text{on} \quad \partial\Omega. \end{array}\right. \tag{3.14}$$

The associated first eigenvalue can be defined as

$$\lambda_1 = \frac{\int_\Omega \alpha M(u)\cdot\nabla\nabla u}{\int_\Omega \rho|u|^2}, \tag{3.15}$$

being u solution of (3.14). The topological derivative of $J(\mathcal{D}) := \lambda_1^{-1}$ is given by

$$D_T J = -\frac{\alpha\mathbb{P}M(u)\cdot\nabla\nabla u + (1-\gamma_\rho)\rho\lambda_1|u|^2}{\lambda_1^2\int_\Omega \rho|u|^2}. \tag{3.16}$$

Similarly, the eigenvalue problem of a Reissner-Mindlin model of a clamped thick plate under free vibration can be stated as: Find (θ, u) and λ, such that

$$\left\{\begin{array}{rcll} -\operatorname{div}(\alpha M(\theta)) + \beta Q(\theta,u) &=& 0 & \text{in} \quad \Omega\,, \\ \operatorname{div}(\beta Q(\theta,u)) &=& \rho\lambda u & \text{in} \quad \Omega\,, \\ \theta = 0,\ u &=& 0 & \text{on} \quad \partial\Omega\,. \end{array}\right. \tag{3.17}$$

The associated first eigenvalue is defined as

$$\lambda_1 = \frac{\int_\Omega(\alpha M(\theta)\cdot(\nabla\theta)^s + \beta Q(\theta,u)\cdot(\theta-\nabla u))}{\int_\Omega \rho|u|^2}, \tag{3.18}$$

being (θ, u) solution of (3.17). The topological derivative of $J(\mathcal{D}) = \lambda_1^{-1}$ is given by

$$D_T J = -\frac{\alpha\mathbb{P}M(\theta)\cdot(\nabla\theta)^s + \beta PQ(\theta,u)\cdot(\theta-\nabla u) + (1-\gamma_\rho)\rho\lambda_1|u|^2}{\lambda_1^2\int_\Omega \rho|u|^2}. \tag{3.19}$$

In the numerical experiment again we consider both models (Kirchhoff and Reissner-Mindlin) in a hold-all domain Ω given by a clamped square plate of dimensions $(0,1)\times(0,1)\text{m}^2$. The contrast parameters $\gamma_\alpha = \gamma_\beta = \gamma_\rho = 10^{-3}$, Young modulus is $E = 210\text{GPa}$, Poisson ratio $\nu = 0.3$, the plate thickness $h = 0.05\text{m}$. We consider two cases, which are: one concentrated mass at the center of the plate and four concentrated masses located at the centre of each plate quadrant. The problems driven by the Kirchhoff model are labeled as Cases K1 and K2 with one and four concentrated masses, respectively. The problems governed by the Reissner-Mindlin theory are labeled as Cases R1 and R2 also with one and

four concentrated masses, respectively. The penalty parameter is set as $\mu = 1.2$ for the Cases K1 and R1 and $\mu = 1.4$ for the Cases K2 and R2. The non-structural concentrated mass are represented by black dots, as depicted in Fig. 7.

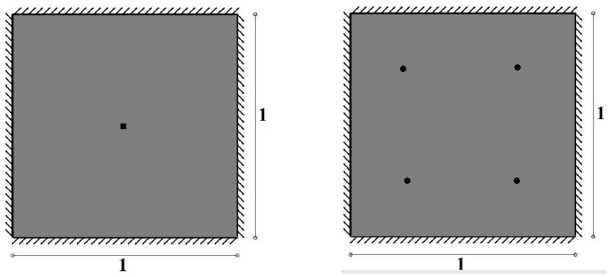

(a) one mass (b) four masses

FIGURE 7. Initial domains with one (a) and four (b) concentrated masses represented by black dots.

.

The optimal topologies for the Kirchhoff hypothesis are shown in Fig. 8. The obtained topologies considering the same initial design and boundary conditions are shown in Fig. 9 for the Reissner-Mindlin hypothesis.

Fig. 10 introduces the normalized first eigenvalue history λ_1/λ_1^0 (where λ_1^0 is its initial value) as the iterative process has evolved. The normalized first eigenvalues history λ_1/λ_2 are introduced in Fig. 11, where the primary axis (left) introduces the results for K1 and R1, while the secondary (right) axis stands for cases K2 and R2, respectively. Cases K2 and R2 presented a higher ratio λ_1/λ_2 when compared to the cases K1 and R1. Based on this results it can be seen that the eigenvalues are most influenced by the position and amount of concentrated mass on the domain than due to the structural hypothesis considered. During the optimization, no coinciding eigenvalue were observed.

The evolution histories for the shape functional and the volume fraction are presented in Figure 12 and Figure 13, respectively. Cases K1 and K2 as well as Cases R1 and R2 presented a quite similar final volume. For the shape function history, the cases K1 and R1, as well as K2 and R2 present similar behavior and final values. It is interesting to highlight that those cases ruled by Reissner-Mindlin hypothesis resulted more conservative concerning to the remaining material when compared to Kirchhoff cases, due to the influence of the transverse shear deformation.

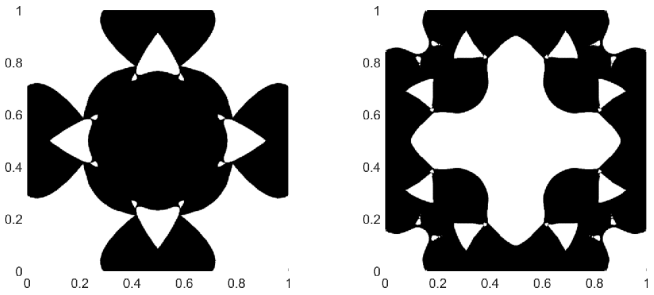

(a) Case K1 (b) Case K2

FIGURE 8. Final topologies for the Kirchhoff problem with one concentrated mass (a) and four concentrated masses (b).

.

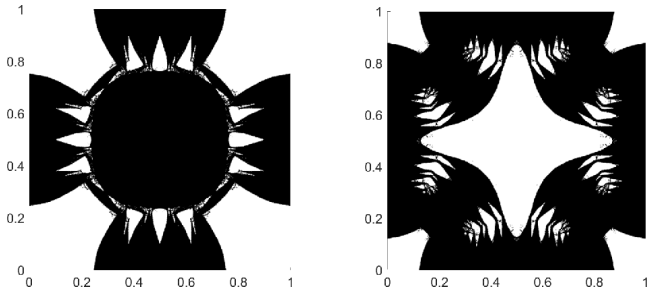

(a) Case R1 (b) Case R2

FIGURE 9. Final topologies for the Reissner-Mindlin problem with one concentrated mass (a) and four concentrated masses (b).

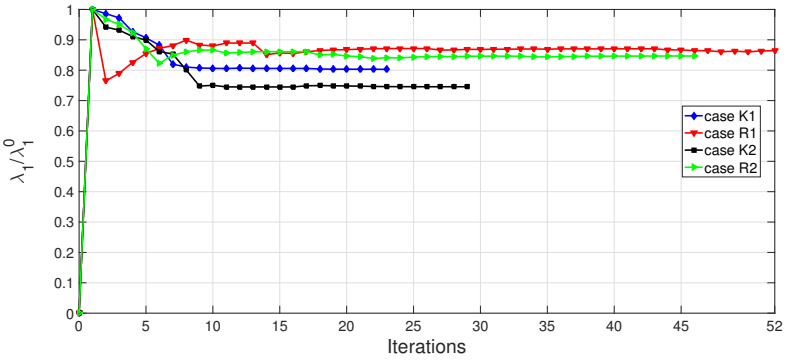

FIGURE 10. Normalized first eigenvalue λ_1/λ_1^0 history.

.

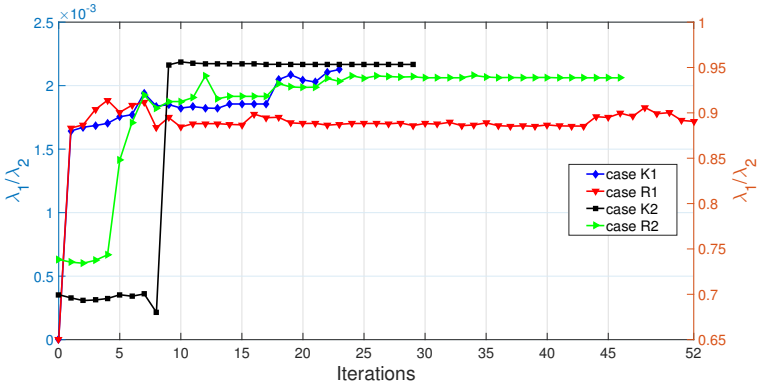

FIGURE 11. Normalized second eigenvalue λ_1/λ_2 history. Cases K1 and R1 left axis and cases K2 and R2 right secondary axis.

.

4. Conclusions

In this paper, the topological derivatives of L^2 and energy norms associated with the solutions to Kirchhoff and Reissner-Mindlin plate bending models, with respect to the nucleation of circular inclusions, have been introduced. In particular, the sensitivities were derived in its closed forms with the help of existing theoretical results. The resulting analytical formulae have been used together with a level-set domain representation method to devise a simple and efficient topology design algorithm. Several finite element-based representative numerical experiments were presented showing its applications in

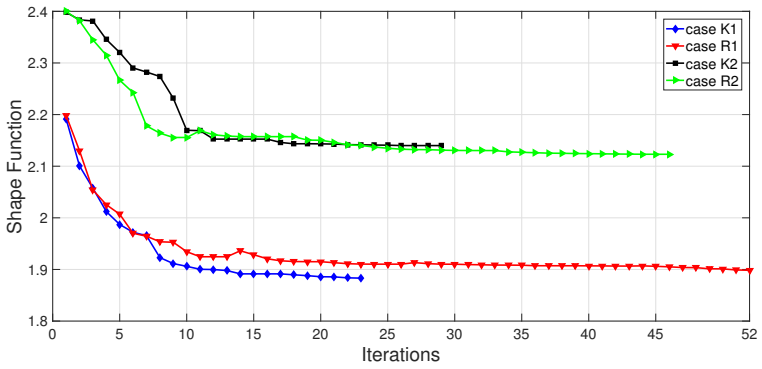

FIGURE 12. Shape function history.

.

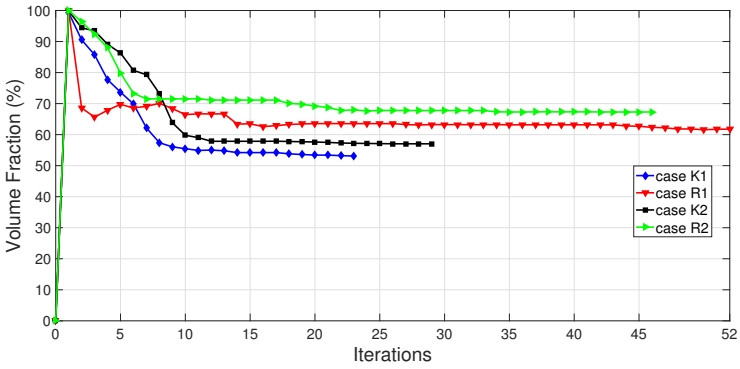

FIGURE 13. Volume fraction history.

.

the context of compliance minimization and eigenvalue maximization of Kirchhoff as well as Reissner-Mindlin plate structures under bending effects.

In the case of compliance minimization, the obtained topologies for the Kirchhoff and Reissner-Mindlin plate bending models are remarkably different, as expected, mainly in the presence of the elastic support. This difference can be explained by the influence of the shear deformation acting on the elastic support. In addition, from a quantitative point of view, the effect of the transverse shear deformations contributes to the compliance value for the Reissner-Mindlin model during the optimization procedure, by capturing the concentrated load effects. As expected, this effect is not observed in the case of Kirchhoff plates.

For the eigenvalue maximization, it could be concluded that the optimal topologies are most influenced by the position and amount of concentrated mass on the domain than due to the structural hypothesis considered. During the optimization process, no coinciding first and second eigenvalues was observed (independently of the plate model considered). The obtained results ruled by Reissner-Mindlin hypothesis resulted more conservative concerning the remaining material when compared to Kirchhoff cases, due to the influence of the transverse shear deformation.

However, it is important to point out that the above comparison between the plates models is far from being exhaustive. Actually, some selected numerical experiments have been presented just to show the robustness and efficiency of the proposed method in solving topology optimization problems in the context of plate bending models.

Acknowledgements

This research was partly supported by CNPq (Brazilian Research Council), CAPES (Brazilian Higher Education Staff Training Agency) and FAPERJ (Research Foundation of the State of Rio de Janeiro). The support is gratefully acknowledged.

Conflict of interest

The authors declare that they have no conflict of interest.

Replication of results

The authors are agreeable to share the codes and details of results with those who contact them.

References

G. Allaire, S. Aubry, and F. Jouve. Eigenfrequency optimization in optimal design. *Computer Methods in Applied Mechanics and Engineering*, 190(28):3565–3579, 2001.

H. Ammari and A. Khelifi. Electromagnetic scattering by small dielectric inhomogeneities. *Journal de Mathématiques Pures et Appliquées*, 82:749–842, 2003.

S. Amstutz. Augmented Lagrangian for cone constrained topology optimization. *Computational Optimization and Applications*, 49:101–122, 2011a.

S. Amstutz. Analysis of a level set method for topology optimization. *Optimization Methods and Software*, 26(4-5):555–573, 2011b.

S. Amstutz and H. Andrä. A new algorithm for topology optimization using a level-set method. *Journal of Computational Physics*, 216(2):573–588, 2006.

S. Amstutz and A.A. Novotny. Topological asymptotic analysis of the Kirchhoff plate bending problem. *ESAIM - Control, Optimisation and Calculus of Variations*, 17(3): 705–721, 2011.

C.T.M. Anflor, K.L. Teotônio, and J.N.V. Goulart. Structural optimization using the boundary element method and topological derivative applied to a suspension trailing arm. *Engineering Optimization*, 50(10):1662–1680, 2018.

D. Bojczuk and Z. Mróz. Topological sensitivity derivative and finite topology modifications: application to optimization of plates in bending. *Structural and Multidisciplinary Optimization*, 39(1):1–15, 2009.

D. Bojczuk and Z. Mróz. Topological sensitivity derivative with respect to area, shape and orientation of an elliptic hole in a plate. *Structural and Multidisciplinary Optimization*, 45(2):153–169, 2012.

D. E. Campeão, S. M. Giusti, and A. A. Novotny. Topology design of plates consedering different volume control methods. *Engineering Computations*, 31(5):826–842, 2014.

S. Czarnecki and T. Lewiński. On minimum compliance problems of thin elastic plates of varying thickness. *Structural and Multidisciplinary Optimization*, 48(1):17–31, 2013.

A.R. Diaaz and N. Kikuchi. Solutions to shape and topology eigenvalue optimization problems using a homogenization method. *International Journal for Numerical Methods in Engineering*, 35(7):1487–1502, 1992.

J. Du and N. Olhoff. Topological design of freely vibrating continuum structures for maximum values of simple and multiple eigenfrequencies and frequency gaps. *Structural and Multidisciplinary Optimization*, 34(2):91–110, 2007.

S. Goo, S. Wang, J. Hyun, and J. Jung. Topology optimization of thin plate structures with bending stress constraints. *Computers & Structures*, 175:134–143, 2016.

R. T. Haftka and Z. Gürdal. *Elements of structural optimization*. Kluwer, Dordrecht, third edition, 1992.

J. Hur, P. Kang, and S.K. Youn. Topology optimization based on spline-based mesh free method using topological derivatives. *Journal of Mechanical Science and Technology*, 31(5):2423–2431, 2017.

W. Khan, B. Ullah, Z. Ullah, et al. The localized radial basis functions for parameterized level set based structural optimization. *Engineering Analysis with Boundary Elements*, 113:296–305, 2020.

G. Kirchhoff. Über das gleichgewicht und die bewegung einer elastischen scheibe. *Journal für Reine und Angewandte Mathematik*, 40:51–88, 1850.

D. Kropiowska, L. Mikulski, and P. Szeptyński. Optimal design of a kirchhoff-love plate of variable thickness by application of the minimum principle. *Structural and Multidisciplinary Optimization*, 59(5):1581–1598, 2019.

R.P. Leal and C.A.M. Soares. Mixed elements in the optimal design of plates. *Structural optimization*, 1(2):127–136, 1989.

S.L. Li, S.Y. Long, and G.Y. Li. A topology optimization of moderately thick plates based on the meshless numerical method. *Computer Modeling in Engineering and Sciences (CMES)*, 60(1):73, 2010.

Q.Q. Liang. *Performance-based Optimization of Structures*. Spon Press, London, 2004.

Q.Q. Liang, Y.M. Xie, and G.P. Steven. A performance index for topology and shape optimization of plate bending problems with displacement constraints. *Structural Multidisciplinry Optimization*, 21(5):393–399, 2001.

R.D. Mindlin. Influence of rotary inertia and shear on flexural motions of isotropic, elastic plates. *Journal of Applied Mechanics ASME*, 18:31–38, 1951.

S. A. Nazarov and J. Sokołowski. Spectral problems in the shape optimisation. Singular boundary perturbations. *Asymptotic Analysis*, 56(3-4):159–204, 2008.

L.C. Neches and A.P. Cisilino. Topology optimization of 2D elastic structures using boundary elements. *Engineering Analysis with Boundary Elements*, 32(7):533–544, 2008.

A. A. Novotny and J. Sokołowski. *Topological derivatives in shape optimization*. Interaction of Mechanics and Mathematics. Springer-Verlag, Berlin, Heidelberg, 2013.

A. A. Novotny, R. A. Feijóo, C. Padra, and E. Taroco. Topological derivative for linear elastic plate bending problems. *Control and Cybernetics*, 34(1):339–361, 2005.

A. A. Novotny, J. Sokołowski, and A. Żochowski. *Applications of the topological derivative method*. Studies in Systems, Decision and Control. Springer Nature Switzerland, 2019.

E. Reissner. The effect of transverse shear deformation on the bending of elastic plates. *Journal of Applied Mechanics ASME*, 12:A69–A77, 1945.

V. Sales, A.A. Novotny, and J.E. Muñoz-Rivera. Energy change to insertion of inclusions associated with the Reissner-Mindlin plate bending model. *International Journal of Solids and Structures*, 59:132–139, 2015.

A.P. Seyranian, E. Lund, and N. Olhoff. Multiple eigenvalues in structural optimization problems. *Structural optimization*, 8(4):207–227, 1994.

J. Sokolowski and A. Zochowski. On the topological derivative in shape optimization. *SIAM Journal on Control and Optimization*, 37(4):1251–1272, 1999.

A. J. Torii and J. Rocha de Faria. Structural optimization considering smallest magnitude eigenvalues: a smooth approximation. *Journal of the Brazilian Society of Mechanical Sciences and Engineering*, 39(5):1745–1754, 2017.

I. Turevsky, S. H. Gopalakrishnan, and K. Suresh. An efficient numerical method for computing the topological sensitivity of arbitrary-shaped features in plate bending. *International Journal for Numerical Methods in Engineering*, 79(13):1683–1702, 2009.

A.G. Weldeyesus and M. Stolpe. Free material optimization for laminated plates and shells. *Structural and Multidisciplinary Optimization*, 53(6):1335–1347, 2016.

Z. Zhang, W. Chen, and X. Cheng. Sensitivity analysis and optimization of eigenmode localization in continuum systems. *Structural and Multidisciplinary Optimization*, 52: 305–317, 2015.

(F.S. Carvalho, D. Ruscheinsky, C.T.M. Anflor) Group of Experimental and Computational Mechanics, University of Brasilia, Gama, Brazil
Email address: {dirlei,fscarvalho}@uft.edu.br, anflor@unb.br

(S.M. Giusti) Universidad Tecnológica Nacional, Facultad Regional Córdoba UTN-FRC / CONICET, Maestro M. López esq. Cruz Roja Argentina, X5016ZAA - Córdoba, Argentina.
Email address: sgiusti@frc.utn.edu.ar

(A.A. Novotny) Laboratório Nacional de Computação Científica LNCC/MCT, Coordenação de Métodos Matemáticos e Computacionais, Av. Getúlio Vargas 333, 25651-075 Petrópolis - RJ, Brasil
Email address: novotny@lncc.br